Stochastic modelling of cross-flow vortex-induced vibrations

J. V. Ulveseter, M. J. Thorsen, S. Sævik, C. M. Larsen

7491 Trondheim, Norway, Department of Marine Technology, Norwegian University of Science and Technology

Abstract

Semi-empirical models are commonly used to predict vortex-induced vibrations (VIV). Empirical parameters are often based on forced harmonic motion tests of short rigid cylinders in one degree of freedom, which is a significant simplification of the three dimensional VIV experienced by flexible cylinders. Still, the models may provide satisfactory estimates of the response of slender marine structures exposed to current. At least in terms of root mean square (r.m.s.) of displacements and strains, dominating frequency and dominating mode. However, VIV of long slender beams, especially in sheared current, show large response variability in time and space, which appears to be of a random nature. Semi-empirical models that predict steady-state VIV are hence unable to reflect the non-stationary response observed in experiments, even though the time and space averaged result might be well represented.

In this work, a previously published semi-empirical time domain model for cross-flow vortex-induced vibrations is modified to describe the stochastic nature of the response of long slender beams subjected to stationary current. The mean non-dimensional frequency of the synchronization model (previously constant) is taken to be a simplified Gaussian process, where standard deviation and spectral frequencies are input. The stochastic synchronization model allows the response to jump between different eigenfrequencies and corresponding modes, and still predict mean and r.m.s. values close to the deterministic model. Its performance is verified through simulation of an experiment with a long riser in sheared flow. The response sensitivity of standard deviation and spectral frequencies is investigated. It indicates that for a proper choice of empirical coefficients, the chaotic response of the riser can be quite realistically simulated in terms of frequency variation and, to some extent, amplitude modulation.

Keywords: Stochastic analysis, time domain simulation, vortex-induced vibrations

1. Introduction

Slender marine structures, such as anchor lines, risers and pipelines, need sufficient structural integrity in order to withstand forces induced by the ocean environment. As oil and gas exploration moves into deeper waters, ocean currents may become the main force contributor. When the current show a sufficient degree of stationarity, shear forces between the body surface and external flow will lead to flow separation and vortex shedding. The consequence is high frequency response, known as vortex-induced vibrations (VIV), acting to lower the fatigue life of slender structures significantly. It is hence important to have accurate VIV prediction tools in structural design.

Even though a flexible slender structure exposed to a time independent current may seem like a fairly simple problem to address, extensive research tells a different story. The difficulty rise from a complex vortex shedding process which is highly three dimensional and turbulent even at fairly low Reynolds number. In addition, interaction between structural response and hydrodynamics makes the vortex shedding process completely different from that of a stationary structure. More than a decade ago, Sarpkaya (2004) found that the experimental focus of VIV researchers was still on flexibly mounted rigid cylinders restricted to move in cross-flow only. Since then, several experiments with flexible pipes both in uniform and sheared current have been conducted (Øritsland, 2004; Braaten and Lie, 2005; Wang et al., 2014), allowing for complicated phenomena such as multi-mode vibrations, combination of standing and travelling waves, interaction between cross-flow and in-line motion causing higher harmonics, and time and space variations in the response process (Wu et al., 2012). Realistic modelling of the latter is the topic of this paper.

Time and space variability of high mode VIV has been experimentally examined by several authors. Modarres-Sadeghi et al. (2011) utilized data from experiments by the Norwegian Deepwater Programme (NDP) of long slender risers (Braaten and Lie, 2005), separating the response into three branches. The VIV could be entirely quasi-periodic with statistically stationary properties, in the sense that one frequency and mode occupied the entire structure for the whole time window, typically in combination with higher harmonics. Observations of other time signals showed a response consisting of time intervals of periodic motion, and other periods of chaotic response with a broad frequency spectrum and no clear peak frequency. The last branch of VIV was seen to be purely chaotic, without time windows of quasi-periodic motion. The variability of high mode VIV was also recognized by Baarholm et al. (2006), after post-processing of experimental data from a large-scale model test of a tensioned riser.

From the previous discussion, it is clear that high mode VIV of flexible pipes behaves rather chaotic, which suggests that prediction tools should be stochastic rather than deterministic. By Swithenbank (2007), a concept called time sharing was introduced as a method to improve reliability of VIV prediction tools, such as SHEAR7 (Vandiver and Li, 2005) and VIVANA (Passano et al., 2014). The intention was to model time variability of dominating frequency, rather than a constant spatial variation, in cases where several natural frequencies were in range of excitation. Time sharing can be considered as a step towards stochastic modelling of VIV. However, it predicts periodic stationary response in the sense that the riser jumps straight from one frequency to another, and the time at each frequency is predefined. To quantify the length of the time intervals associated with each frequency, and how the vibration amplitude depends on frequency variability, Swithenbank and Larsen (2012) used laboratory tests of a riser in uniform and sheared flow. As one single frequency would dominate a large portion of the pipe, high amplitude VIV was seen. When the dominating frequency experienced a shift in time, a multi-frequency response would develop, associated with a drop in amplitude of vibration. Swithenbank and Larsen (2012) concluded that the energy contained in the system was a main driving factor in determining the duration of high and low amplitude state.

There has been other attempts to model the stochastic nature of VIV. For instance, a van der Pol wake oscillator with a random spatial parametric variation was developed by Mukundan et al. (2009), in order to predict fatigue damage for the NDP experiments. This stochastic prediction tool was able to provide a rough estimate of fatigue damage found directly from the measurements. Lie et al. (2008) proposed a method for analysis of combined cross-flow and in-line response, using a time sharing approach combined with a stochastic model of displacement amplitudes. The method was based on frequency domain analysis and could potentially include the effect of higher harmonics in addition to the fundamental frequency. However, the method needed data from experiments with simultaneous cross-flow and in-line VIV, which was not available at the time of publication.

The starting point of the stochastic VIV analysis presented below is a previously published semi-empirical time domain model. It has shown to produce realistic estimates of the structural response through simulation of several experiments of flexible pipes in uniform, sheared and oscillatory flow (Thorsen et al., 2014, 2015, 2016). Recently, heave induced VIV of an SCR with non-linear bottom contact was simulated. The response was in good agreement with measurements (Thorsen et al., 2017). The fundamental idea of the model is the way synchronization between hydrodynamic force and response is handled. For a (constant) range of non-dimensional frequencies, the hydrodynamic force will synchronize with the structural velocity providing a positive energy transfer from the water to the structure.

In this paper, the original semi-empirical time domain model is referred to as deterministic, and the new model as stochastic. The stochastic feature is to make the mid-point of the synchronization range a slowly time-varying Gaussian process. This allows the flexible pipe to shift between eigenfrequencies and their corresponding modes, in an attempt to model time and space variability measured in high mode VIV experiments. The stochastic process introduces two new empirical coefficients, i.e. the standard deviation and the upper limit of spectral frequencies included in the process. Sheared flow experiments with a bare riser from the NDP tests are used to verify the new stochastic approach against the measurements. Response sensitivity of the two new empirical coefficients is performed, trying to realistically capture both amplitude modulation and frequency variations the riser experiences.

2. Deterministic hydrodynamic force model

The hydrodynamic loading per unit length was by Thorsen et al. (2017) defined as:

$$\mathbf{F}_n = C_M \rho \frac{\pi D^2}{4} \dot{\mathbf{u}}_n - (C_M - 1)\rho \frac{\pi D^2}{4} \ddot{\mathbf{x}}_n + \frac{1}{2}\rho D C_D |\mathbf{v}_n| \mathbf{v}_n + \frac{1}{2}\rho D C_v |\mathbf{v}_n| (\mathbf{j}_3 \times \mathbf{v}_n) \cos\phi_{\text{exc}}. \tag{1}$$

The three first terms of equation 1 are the well-know Morison's equation acting in the cross-section plane (neglecting forces in the longitudinal direction). The last term describes the effect of vortex shedding, and is applied perpendicular to the normal component of the relative velocity (i.e. the instantaneous cross-flow direction). The parameters and variables are defined according to the following list, with coordinate system for a cylinder strip as illustrated in figure 1.

- C_M: Inertia coefficient from Morison's equation.
- C_D: Drag coefficient from Morison's equation.
- C_v: Dimensionless coefficient representing the magnitude of the vortex shedding force.
- $\dot{\mathbf{u}}_n$: Water particle acceleration normal to the cylinder.
- $\ddot{\mathbf{x}}_n$: Cylinder acceleration normal to the cylinder.
- $\mathbf{v}_n$: Relative flow velocity normal to the cylinder. The relative velocity is found as $\mathbf{v} = \mathbf{u} - \dot{\mathbf{x}}$.

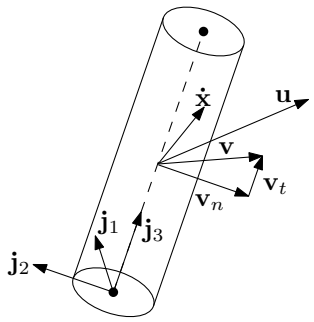

Figure 1: A cylinder segment with local coordinate system and velocity vectors (Thorsen et al., 2017).

The Morison's equation consists of an inertia term and a drag term. The latter provides hydrodynamic damping in the cross-flow direction, and the first term determines added mass properties. The vortex shedding forcing term is added to Morison's equation to cause excitation under what commonly is referred to as "lock-in"-conditons. Thorsen et al. (2017) acknowledged that Morison's drag force might be inaccurate as damping model in case of VIV. However, it is the total energy balance between damping and excitation which is of main concern. Hence, by picking C_v (excitation) relative to the drag coefficient (damping), it is possible to obtain a realistic level of energy transfer between the water and the structure, to ensure the self-limiting properties of VIV.

A synchronization model is utilized to model lock-in. The fundamental idea is that the frequency of the vortex shedding force may vary in time, and the variation depends on the response of the structure. More specifically, the instantaneous frequency of the vortex shedding force, $\dot{\phi}_{\text{exc}}$, is calculated from the phase difference between the structural velocity component in the instantaneous cross-flow direction, $\phi_{\dot{y}_{\text{rel}}}$, and the force itself, ϕ_{exc}:

$$\frac{d\phi_{\text{exc}}}{dt} = 2\pi f_{\text{exc}} = \frac{2\pi |\mathbf{v}_n|}{D} \hat{f}_{\text{exc}}, \tag{2}$$

where

$$\hat{f}_{\text{exc}} = \hat{f}_0 + \Delta \hat{f} \sin(\phi_{\dot{y}_{\text{rel}}} - \phi_{\text{exc}}). \tag{3}$$

$\hat{f}_{\text{exc}}$ determines the range of non-dimensional frequencies where synchronization is possible. When the structural response fulfils the synchronization requirements, energy is transferred from the water to the structure.

$\hat{f}_0$ and $\Delta\hat{f}$ determines the mean value and the "amplitude" of the synchronization range, respectively. They are both empirically determined, with default values $\hat{f}_0 = 0.18$ and $\Delta\hat{f} = 0.08$. The component of the structural velocity in the instantaneous cross-flow direction is calculated from:

$$\dot{y}_{\text{rel}} = \dot{\mathbf{x}} \cdot \frac{\mathbf{j}_3 \times \mathbf{v}_n}{|\mathbf{v}_n|}. \tag{4}$$

To implement the synchronization model in a time domain simulation of vortex-induced vibrations, $\phi_{\dot{y}_{\text{rel}}}$ must be numerically approximated at every time step and every node. Thorsen et al. (2017) proposed a method based on a phase portrait (see figure 2). Structural velocity in the instantaneous cross-flow direction is normalized by its r.m.s. value, which is approximated by

$$\sigma_{\dot{y}_{\text{rel}}}(t_i) = \sqrt{\frac{n_m - 1}{n_m}(\sigma_{\dot{y}_{\text{rel}}}(t_{i-1}))^2 + \frac{1}{n_m}(\dot{y}_{\text{rel}}(t_i))^2}. \tag{5}$$

t_i is the current time step and t_{i-1} is the previous time step. n_m is a parameter which approximates how many previous time steps the current r.m.s. value is calculated from. The default value is $n_m = 500$. An equivalent procedure is used to find the r.m.s. value of the structural acceleration.

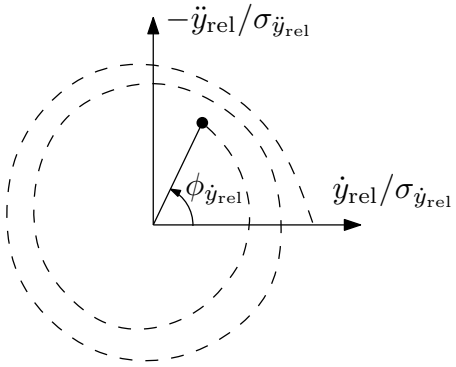

Figure 2: The phase diagram illustrates how the instantaneous phase of the relative cross-flow velocity is found (Thorsen et al., 2017).

3. Stochastic Synchronization

To model the random nature of high mode VIV, the synchronization model is modified. According to equation 3, the synchronization range is constant (since $\hat{f}_0$ and $\Delta\hat{f}$ are constants). The new approach keeps $\Delta\hat{f}$ unchanged, but $\hat{f}_0$ now converges towards a Gaussian process as the length of the time domain simulation approaches infinite (visualized in figure 3). The reason for this particular choice is that the Gaussian distribution is simple to work with and it is symmetric about its mean value. Hence local maxima and minima have same portability of occurrence, with equal distance away from the mean value. To verify that the synchronization range is a Gaussian process, or alternatively to substitute it with a more realistic distribution, hydrodynamic force measurements of flexible pipes experiencing stochastic VIV are demanded. As such data are missing for the experiment which is simulated below, and because the present formulation is an initial attempt, no more effort has been made to experimentally verify the probabilistic distribution of $\hat{f}_0$. Instead, this paper focuses on the structural response induced by the stochastic hydrodynamic force model, and how it compares to the deterministic approach and response measurements.

In the following, capital letters symbolises stochastic variables, meaning that the random process $\hat{f}_0$ is named $\hat{F}_0$, to easily distinguish between them. The stochastic process is defined by:

$$\hat{F}_0(t) = \sum_{i=1}^{N_f} \hat{f}_{0\text{a},i} sin(\phi_{\text{stoc},i}) + \hat{f}_0 \tag{6}$$

where

- $\phi_{\text{stoc},i}$ is the instantaneous phase of frequency component i.
- $\hat{f}_0$ is the mean value of the process (equal to the deterministic value).
- N_f is the number of frequency components included.
- $\omega_i = d\phi_{\text{stoc},i}/dt = 2\pi\hat{f}_i|\mathbf{v}_n|/D$ is frequency component i of the process.
- $\hat{f}_{0\text{a},i} = \sqrt{2S_{\hat{F}_0\hat{F}_0}(\omega_i)\Delta\omega}$ is the amplitude of frequency component i.
- $\Delta\omega = 2\pi\Delta\hat{f}|\mathbf{v}_n|/D$ is the length of a frequency interval.

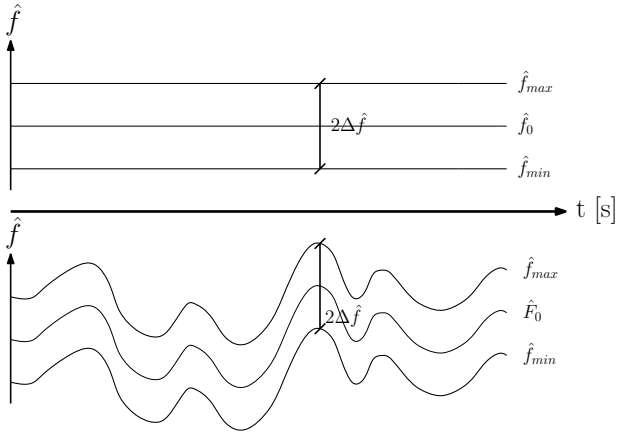

Figure 3: How the synchronization range develops in time. Upper: Deterministic approach. Lower: Stochastic approach.

$\hat{F}_0$ varies systematically around the value of $\hat{f}_0$, implying that on average, the stochastic model will display a similar synchronization range as presented in section 2. The standard deviation of the process, $\sigma_{\hat{F}_0\hat{F}_0}$, is determined from the energy spectrum $S_{\hat{F}_0\hat{F}_0}$. For simplicity, the spectrum is assumed to be constant with a given frequency range, according to figure 4. The spectrum area equals the variance $\sigma^2_{\hat{F}_0\hat{F}_0}$, determining the amplitude of the instantaneous mean value of the synchronization range. The maximum spectral frequency is governed by the value of c (see figure 4). If c is large, the stochastic process will display rapid time fluctuations, and vice versa. The general idea is that $\hat{F}_0$ shall be slowly varying relative to the instantaneous frequency of VIV. Then, the response has time to build up before the synchronization region changes so that other eigenfrequencies with their respective modes might be excited. Hence $c << 1$.

The mathematical formulation of the stochastic process in equation 6 deviates from what typically applied as a simplified Gaussian distribution in linear wave theory. The instantaneous wave elevation is, by Fergestad and Løtveit (2014), given by $\xi(t) = \sum_{i=1}^{N_f} \xi_{a,i} sin(\omega_i t - \epsilon_i)$, where ϵ_i is a stochastic phase uniformly distributed between 0 and 2π. In the present work, the instantaneous phase $\phi_{\text{stoc},i}$ substitutes the more well-know formulation $\omega_i t - \epsilon_i$, consistent with the deterministic synchronization model presented in section 2. The reason is that the stochastic process in equation 6 is controlled by non-dimensional frequencies. The conversion to real frequencies introduces a scaling factor proportional to $|\mathbf{v}_n|/D$. For a stationary current, a cylinder vibrating in both cross-flow and in-line directions will have a fluctuating relative velocity according to $|\mathbf{v}_n(t)| = \sqrt{(U - \dot{x}(t))^2 + \dot{y}(t)^2}$, where $\dot{x}$ and $\dot{y}$ are the in-line and cross-flow structural velocities, respectively. If the standard way of dealing with frequencies was applied (as for linear wave theory), the slowly varying stochastic process would experience high frequency noise due to time variations of $|\mathbf{v}_n|$ (see figure 5). By making $\phi_{\text{stoc},i}(t = 0)$ randomly distributed between 0 an 2π for all the frequency components, the wanted probability distribution is obtained without any noise. Simulations are performed with $N_f = 100$ in order to verify that $\hat{F}_0$ actually converges towards a Gaussian process with wanted mean value and standard deviation. Results of several simulations are plotted as a histogram and compared to the probability density function of a normal distribution with same parameters in figure 6. The comparison indicate that $N_f = 100$ is sufficient. Hence all subsequent analyses have been performed with 100 frequency components.

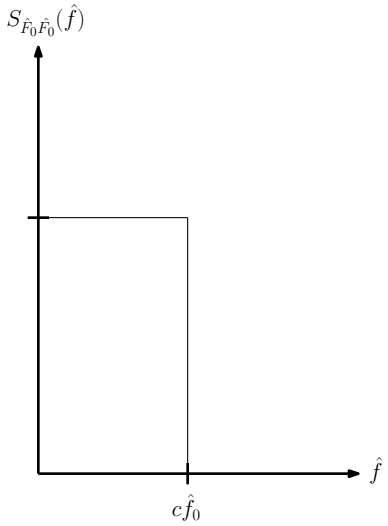

Figure 4: Spectrum of stochastic process $\hat{F}_0$.

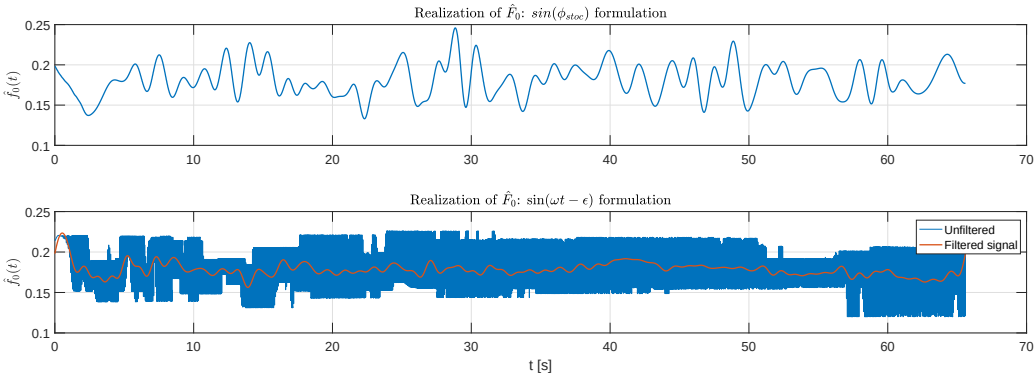

Figure 5: Upper: Realization of $\hat{F}_0(t) = \sum_{i=1}^{N_f} \hat{f}_{0a,i} sin(\phi_{stoc,i}) + \hat{f}_0$ Lower: Realization of $\hat{F}_0(t) = \sum_{i=1}^{N_f} \hat{f}_{0a,i} sin(\omega_i t - \epsilon_i) + \hat{f}_0$.

3.1. Discussion of stochastic properties

To provide an indication of the amount of variability to be expected when applying a stochastic synchronization range, properties of $\hat{F}_0$ and its effect on the response of long slender beams, are discussed. In the following, F_x symbolises the cumulative probability distribution of a variable x, and f_x is its density function. As a simplification, the process $\hat{F}_0$ is assumed to be Gaussian, narrow-banded and stationary. Then, the individual maxima (i.e. amplitudes) will follow a Rayleigh distribution. Its probability density function (pdf) is given by:

$$\mathrm{f}_{\hat{F}_{0,m}}(\hat{f}_a) = \frac{\hat{f}_a}{\sigma^2_{\hat{F}_0\hat{F}_0}} \exp(-\frac{\hat{f}_a^2}{2\sigma^2_{\hat{F}_0\hat{F}_0}}). \tag{7}$$

The largest amplitude expected among N is expressed as:

$$\hat{f}_a = \int_0^\infty \mathrm{f}_{\hat{F}_{0,lm}}(\hat{f})\hat{f}d\hat{f}, \tag{8}$$

where $\mathrm{f}_{\hat{F}_{0,lm}}$ is the pdf of the largest maxima out of N, assuming statistically independent amplitudes and that they are all identically Rayleigh distributed:

$$\mathrm{f}_{\hat{F}_{0,lm}}(\hat{f}_a) = \mathrm{N}[\mathrm{F}_{\hat{F}_{0,m}}(\hat{f}_a)]^{\mathrm{N}-1}\mathrm{f}_{\hat{F}_{0,m}}(\hat{f}_a). \tag{9}$$

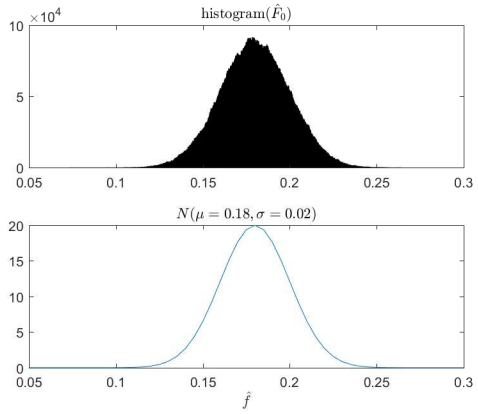

Figure 6: Upper: Histogram of $\hat{F}_0$ from simulations. Lower: Pdf of Gaussian distribution with $\mu = 0.18$ and $\sigma = 0.02$.

Equation 7 and 8 are plotted in figure 7, for different values of $\sigma_{\hat{F}_0\hat{F}_0}$. The figures indicate how much the synchronization range is able to shift. Choosing a standard deviation of 0.02, assuming the mean value $\hat{f}_0 = 0.18$, the most probable shift has an amplitude of 0.02, i.e. around 11 % change relative to the deterministic synchronization range. By looking at the largest shift among N maxima, the centre of the synchronization range may change by approximately 0.05 units as N approaches 20. This implies a relative change of synchronization frequencies by almost 30%.

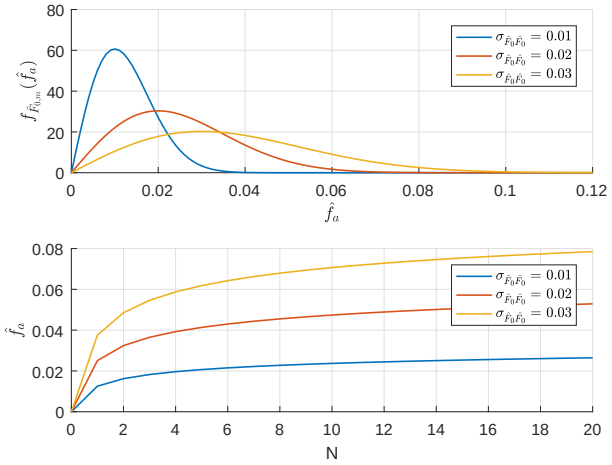

Figure 7: Approximate statistical properties of $\hat{F}_0$ for different standard deviations. Upper: Pdf of amplitudes. Lower: Expected maximum amplitude out of N.

It is important to have in mind that the hydrodynamic force model applies a strip theory formulation. For every translation degree of freedom along a flexible structure exposed to VIV, the stochastic processes determining the synchronization range are independent. Said differently, there is no communication between the $\hat{F}_0(t)$'s at the different nodes. Thus, the range of dominating frequencies displayed by a flexible pipe is not governed by the maximum/minimum value of $\hat{F}_0$ at one specific node, but rather how they correlate in time. That being said, numerical tests indicate that a mode shift can be induced from stochastic variation at only a small fraction of the pipe length. The value of $\hat{f}_a$ that governs the response is hence difficult to predict. In the following it is assumed that $\hat{f}_a = 0.04$ is representative for the maximum response variation the pipe might experience for $\sigma_{\hat{F}_0\hat{F}_0} = 0.02$. If another standard deviation is utilized, $\hat{f}_a$ is assumed to scale linearly. To summarize, the governing amplitude of frequency variability for a flexible pipe is assumed to be given by $\hat{f}_a = 2\sigma_{\hat{F}_0\hat{F}_0}$.

The question is then: By how much does the governing value of $\hat{f}_a$ affect the range of frequencies a flexible pipe might respond? As an illustrative example, the bare riser in sheared flow analysed in section 5 is considered. A (linear) finite element model is made, providing the natural frequencies of the structure. For simplicity, still water added mass is assumed, even though the response itself might change the added mass properties quite significantly (see for instance Vikestad et al. (2000)). The same hydrodynamic coefficients as presented in table 2 are utilized (i.e. $\sigma_{\hat{F}_0\hat{F}_0} = 0.016$). To easily convert between $\hat{f}_a$ and f_a, it is assumed that $|\mathbf{v}_n| \approx U$. Thus, in dimension [Hz], the midpoint of the synchronization range might change by $f_a \approx (U/D)\hat{f}_a$. To make the approximation even simpler, the actual still water natural frequency is found from the dominating mode from the deterministic analysis in figure 13. The synchronization range ($2\Delta\hat{f}$) is not taken into consideration, only $\hat{F}_0$.

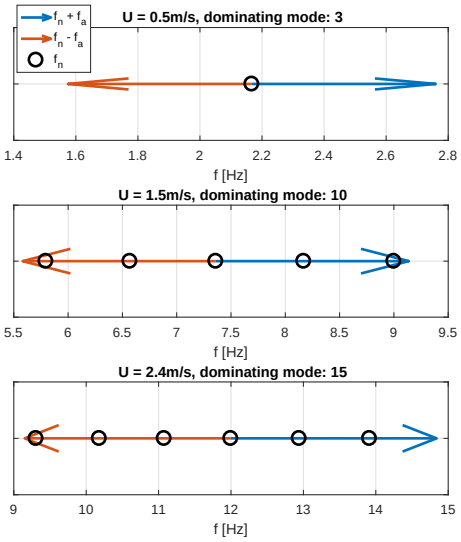

Figure 8: Expected variability of riser response with structural properties given in table 1, for different current velocities. Black circles represent still water natural frequencies which might be induced when $\sigma_{\hat{F}_0\hat{F}_0} = 0.016$.

For current velocity of 0.5 m/s, 1.5 m/s and 2.4 m/s, the result of the above example is presented in figure 8. It shows how many natural frequencies are contained in the expected range of variability (given by $f_n \pm f_a$). The midpoint of each subplot is the still water natural frequency f_n associated with the dominating mode for each current velocity. For U = 0.5 m/s no change of natural frequency is expected to be induced by $\hat{F}_0$, implying that the stochastic and the deterministic model will produce similar results. For U = 1.5 m/s and U = 2.4 m/s several higher and lower natural frequencies are covered by the stochastic synchronization model, which means that the response is expected to vary between these frequencies. Decent agreement with the simulations presented in figure 13 indicates that the above assumptions are fair.

Be aware that the assumptions and conclusions in the example above have no influence on the subsequent analyses. Instead, it should be considered a rough guideline for how to predict expected response variation for a specific choice of $\sigma_{\hat{F}_0\hat{F}_0}$, when natural frequencies of the flexible pipe are known in advance.

4. NDP experiments

As a benchmark study of high mode VIV, Norwegian Deepwater Programme (NDP) conducted a series of towing tests of a long slender riser. Details about the experiment was reported by Braaten and Lie (2005), an the following information is extracted from it. Both uniform and sheared flow was investigated for velocities between 0.3 m/s-2.4 m/s. In order to measure the riser response, 40 and 24 strain gauge transducers were attached to the cylinder surface in in-line and cross-flow directions respectively. In addition, 8 accelerometers in both degrees of freedom were installed. Two strake geometries with several coverage factors were towed,

Table 1: Structural properties of bare riser in the NDP experiments.

Parameter	**Size**
Length (L)	38 m
Diameter (D)	0.027 m
Bending stiffness (EI)	599 Nm^2
Tension (T)	4300-4640 N
Mass per unit length	0.933 kg/m
Young's modulus (E)	$36.2 \cdot 10^9$ $\mathrm{N/m}^2$

in addition to a bare riser configuration. Data from the latter is used to verify the proposed model, and the structural properties are provided in table 1.

Throughout this paper experimental values are separated in two cases. The first case is results obtained after a band-pass filter has removed the effect of higher harmonics, whereas the second one is from the unfiltered measurements.

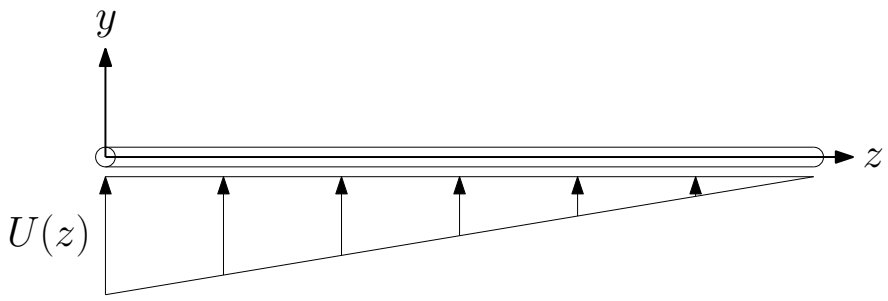

Figure 9: Riser in sheared current.

5. Case study

5.1. Tuning of hydrodynamic coefficients

In order to model the NDP sheared flow experiment of a bare riser (figure 9), the coefficients in the semi-empirical model must be determined. The empirical parameters in Morison equation, i.e. inertia and drag force coefficients, are chosen as $C_D = 1.2$ and $C_M = 2$, which are typical values for circular cylinders in the sub-critical flow regime. The vortex shedding force coefficient C_v is chosen for best fit with experiments by Gopalkrishnan (1993). According to Thorsen et al. (2017), this is for $C_v = 1.2$ (when $C_D = 1.2$). The vortex shedding force will excite vibrations under lock-in conditions, whereas the drag force act as cross-flow damping. $C_v = C_D = 1.2$ has been shown to limit excitation to about an amplitude ratio of 0.8. Hence, if the vibrations exceed this level, energy is transferred away from the structure. No extensive sensitivity study of C_v has yet been published, but the coefficient is assumed to depend on Reynolds number. For simplicity, the latter has not been taken into account, meaning that C_v is constant for all analyses in this paper, regardless of current velocity. For more information about the vortex shedding force coefficient, reference is made to Thorsen et al. (2017). For the deterministic model, the synchronization range is given by $\hat{f}_0$ and $\Delta\hat{f}$. The default values are multiplied with a factor 0.8 to provide a decent match with dominating modes of strain, reported by Braaten and Lie (2005). Hence $\hat{f}_0 = 0.144$ and $\Delta\hat{f} = 0.064$. Synchronization for lower non-dimensional frequencies than the default values indicate that the vortex shedding frequency was lower in the experiment than expected. It is to be noted that the fluid inertia force (first term of equation 1) is zero for all subsequent simulations, because the water particle speed is constant (i.e. $\dot{\mathbf{u}}_n = 0$).

The stochastic synchronization introduces two new empirical coefficients, i.e. $\sigma_{\hat{F}_0\hat{F}_0}$ and c. Recall that the latter determines the frequency of the time variation. A large c is expected to induce more shifts of oscillation frequency for a given time interval, than a low value. The standard deviation $\sigma_{\hat{F}_0\hat{F}_0}$ controls the magnitude of these frequency shifts. A small standard deviation is associated with small changes of oscillation frequency, and vice versa. Finding proper values of $\sigma_{\hat{F}_0\hat{F}_0}$ and c is not straightforward. In the

present study two considerations have been made to determine the stochastic parameters. First, the power spectra obtained from the experimental strain signals have been found. The bandwidth of the spectra relates to $\sigma_{\hat{F}_0\hat{F}_0}$, indicating the span of active frequency components in the time signal. How many local peaks are found within this bandwidth relates to the number of frequency shifts for a given time duration, which is connected to the choice of c. A schematic illustration is provided in figure 10 to explain the idea. It is to be noted that the procedure comes with uncertainty, as both the experimental and stochastic time series are of limited duration. Hence the stochastic model may induce different response for different realisations of the same case. The experimental time series show varying degree of frequency bandwidth for every towing velocity, although the tendency is towards larger frequency bandwidth for increasing velocity (see figure 12). The second consideration used to determine the stochastic parameters relates to experimental findings reported by Lie et al. (2008). In their study, the limit for random response was found to be at about 10th mode and above in uniform and sheared flow. In the present work, "stochastic response" is interpreted as to what conditions the stochastic synchronization range is expected to induce more than one eigenfrequency in the response signal. From these considerations $c = 0.07$ and $\sigma_{\hat{F}_0\hat{F}_0} = 0.016$ are selected. The empirical coefficients are listed in table 2 and they are utilized in subsequent analyses, if not stated otherwise.

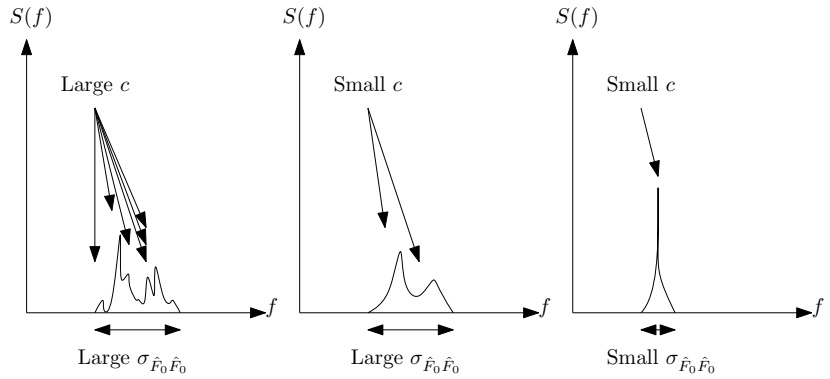

Figure 10: Schematic illustration of power spectra and how they relate to the stochastic parameters c and $\sigma_{\hat{F}_0\hat{F}_0}$, when the time series are of equal length.

Table 2: Hydrodynamic coefficient for sheared flow simulation.

Parameter	**Deterministic**	**Stochastic**
C_v	1.2	1.2
C_D	1.2	1.2
C_M	2	2
$\hat{f}_0$	0.144	0.144
$\Delta\hat{f}$	0.064	0.064
c	-	0.07
$\sigma_{\hat{F}_0\hat{F}_0}$	-	0.016

5.2. Structural and numerical model

The riser is modelled using linear beam elements with in-line and cross-flow translation degrees of freedom, plus rotations, at each node. The mass distribution is consistent (not lumped at each node), and the stiffness has contributions form both bending (EI) and tension (T). Since the experiment contains quite high current velocities, the static drag will significantly increase the tension as the towing speed is increased from zero. It is however assumed that tension variations due to VIV are insignificant, when the towing is steady-state. The mean tension for each run was reported by Brunborg (2013), and these values are used in the linear stiffness formulation to avoid more computational demanding non-linear finite elements. The structural damping is assumed proportional to the stiffness matrix $\mathbf{K}$, i.e. $\mathbf{C} = \alpha\mathbf{K}$, where α is a scalar. For all simulations $\alpha = 10^{-4}$, which provides a structural damping less or equal to 0.4 % of critical, for the range of induced frequencies. The same damping level was found from decay tests by Braaten and Lie (2005).

The equation of motion is solved by the time integration scheme Newmark-β, with parameters matching the method of constant average acceleration (see e.g. Langen and Sigbjoernsson (1979)). Prior to choosing time step length, the dominating frequency of the cross-flow vibrations was extracted from the experiment, for each current speed. From these values, the time increment was chosen to make sure 200 time steps were applied per cross-flow VIV period. For one of the simulations, the time step length was divided by two. The riser response was not affected in any significant way, hence verifying that the initial choice was sufficient. 250 finite elements are used in the simulations presented below. Convergence was verified by performing analyses with twice the mesh refinement, as its influence on the output was minor. A flowchart is provided in figure 11, to summarize the prediction method now that all essential elements of the model have been described.

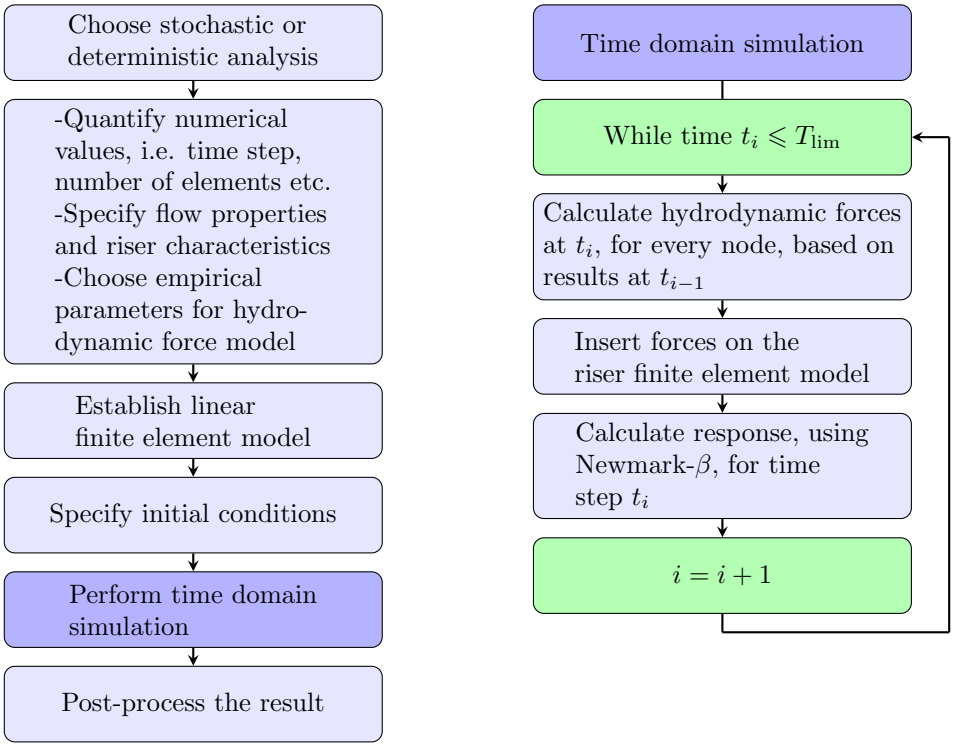

Figure 11: Flow diagram of prediction method. Left: General program flow. Right: Details about time domain simulation.

5.3. Result and discussion

5.3.1. General observations

The model performance as function of current velocity is reported in figure 12, 13, 14 and 15. Dominating frequency (figure 12) is found for all positions along the riser and for all time steps through wavelet analysis. Time and space variability is visualized by shaded areas in the plots. The upper shade limit is the average value of the 1/3 largest dominating frequencies, and correspondingly, the lower limit is given by the mean value of the 1/3 smallest, for all current velocities. From figure 12, it is clear that the experimental results show significant variance which tends to increase for increasing current speed. The stochastic model is able to reproduce this feature, which is seen by comparing the blue and the red shadow in figure 12. In contrast, the deterministic model (black circles) predicts an almost constant dominating frequency for each velocity. In general, the frequency is slightly overpredicted. Recall that the empirical coefficients $\hat{f}_0$ and $\Delta\hat{f}$ where chosen to match dominating mode rather than frequency.

The dominating mode for both the deterministic and stochastic model is found from modal analysis, where the modal weight factors each correspond to a specific mode shape. The idea is that the curvature (proportional to strain) as function of riser position and time can be represented as a sum:

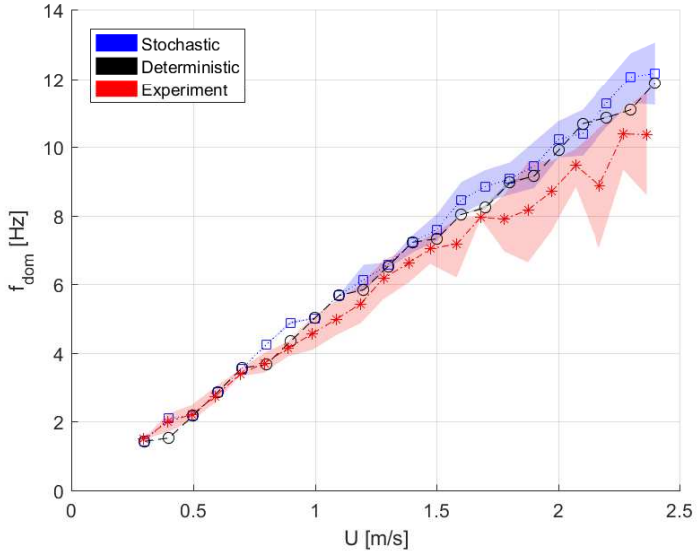

Figure 12: Dominating frequency, sheared flow.

$$\kappa(z,t) = \sum_i \frac{d^2\phi_i(z)}{dz^2} q_i(t). \tag{10}$$

$d^2\phi_i/dz^2$ is the second spatial derivative of the displacement mode shape and $q_i(t)$ is the modal weight factor, both for mode number i. For each time interval of an oscillation cycle, the weight factor experiencing the maximum absolute value, is considered to be the dominating one. Hence, its mode is defined as the dominating mode for that specific time period. The shaded areas in figure 13 give the largest and smallest dominating mode observed over 225 oscillation cycles, for each current velocity. The figure shows that the deterministic model reaches a steady-state response with one dominating mode for all simulations. The stochastic model predicts time changing dominating mode for all current velocities above 1.1 m/s. Two different modes (6 and 7) are seen to dominate already at U=0.9 m/s. However, the frequency variation is almost zero at this particular speed (recall figure 12), which suggests that one of the eigenfrequencies occupy most of the time window. At U= 1.1 m/s, the dominating mode is in range 8-10. The variability is increasing as the current speed is raised. The observed randomness is in good agreement with what found in the literature. Recall that Lie et al. (2008) classified the limit for stochastic response at about 10th mode and above in uniform and sheared flow.

Modal analysis was performed on the NDP strain measurements as well. Even after low and high frequency components were filtered out, noise made the lower strain modal weight factors completely dominating. To determine participating modes Kristiansen and Lie (2005) applied combined modal analysis of strain and acceleration measurements in Fourier space. Their reported dominating modes (for strain) are presented in figure 13 without including variability.

To ensure that the strain amplitudes are predicted with sufficient accuracy, the mean value of r.m.s. of cross-flow strain is reported in figure 14. The experimental values are filtered so that higher order components are excluded (labelled "Experiment 1-ω"). The unfiltered values are also included in the figure. The agreement between the predictions and the filtered measurements is good, indicating that the strength of the vortex shedding force $C_v = 1.2$ provides a decent fit for the whole range of current velocities. Figure 14 shows a moderate variability for the stochastic model (blue shadow). This is achieved by splitting the strain time series into $N_{split} = 5$ equally long periods. Mean r.m.s. of strain is calculated for each of the intervals, and the figure indicate the minimum and maximum value obtained from simulation. The same procedure is applied to the deterministic strain time series, but due to the steady-state response, no variation is seen. It should be noted that the deterministic model predicts slightly larger values than the stochastic model. This is probably because of the random variation in synchronization range, which on average provides a slightly

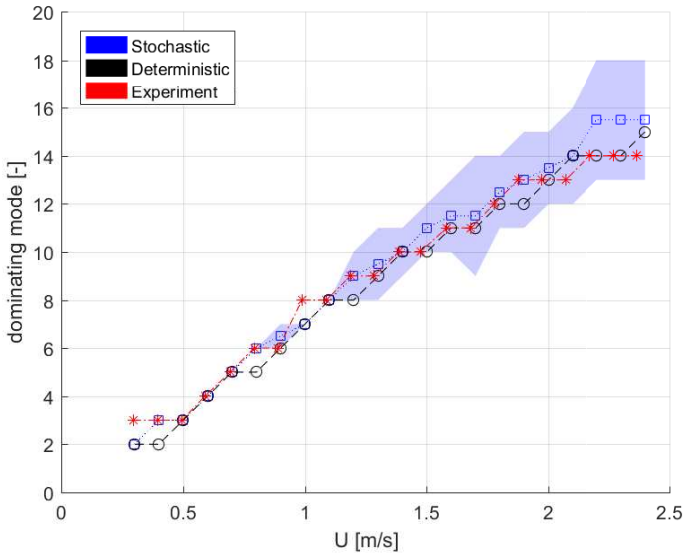

Figure 13: Dominating mode, sheared flow.

smaller energy input to the system. However, the difference is small.

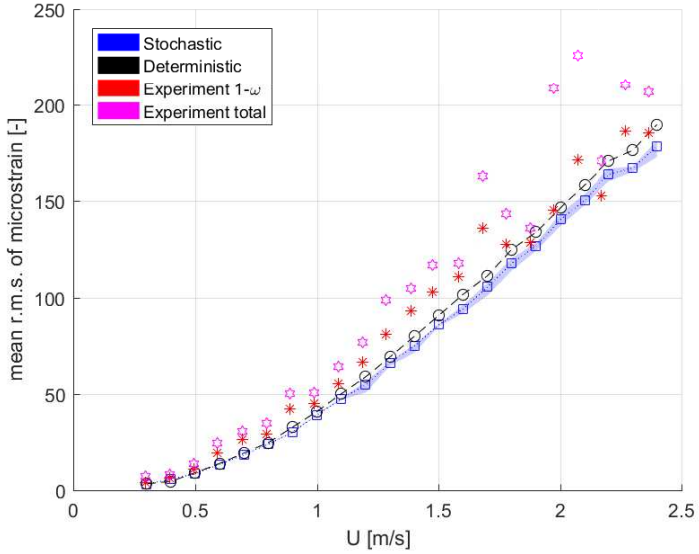

Figure 14: Mean of r.m.s. strain, sheared flow.

The ultimate goal of VIV prediction tools is to provide accurate estimates of fatigue damage. The rainflow counting procedure from the WAFO toolbox in MATLAB has been used to calculate half cycles with corresponding stress ranges, both for simulations and experiments. Time series of longitudinal stress are obtained from the simple relationship $\sigma_{zz} = E\epsilon_{zz}$, where E is Young's modulus, and ϵ_{zz} is axial engineering strain. An SN-curve is chosen to relate each stress range $\Delta\sigma$ with a number of cycles before failure N. According to DNV GL (2014), the following SN-curve applies to a non-welded pipe section without corrosion protection:

$$\log(\mathrm{N}) = 12.436 - 3\log(\Delta\sigma). \tag{11}$$

The Miner-Palmgren relationship is utilized to find the total accumulated fatigue damage:

$$D = \sum_i \frac{n_i}{N_i}, \tag{12}$$

where n_i is number of cycles the structure experiences for stress range $\Delta\sigma_i$, and failure occurs as $D > 1$.

The maximum yearly fatigue damage for each current velocity is plotted in figure 15. For the deterministic and stochastic model, the stress time series are split into $N_{split} = 5$ equally long periods (as for strain), and fatigue is calculated separately for each part. As expected, the stochastic model shows deviations between maximum and minimum fatigue values for high velocities where several frequencies are activated. The deterministic model converges towards a specific value for each current velocity. The trend is that both models are able to provide reasonable estimates of the filtered experimental fatigue damage.

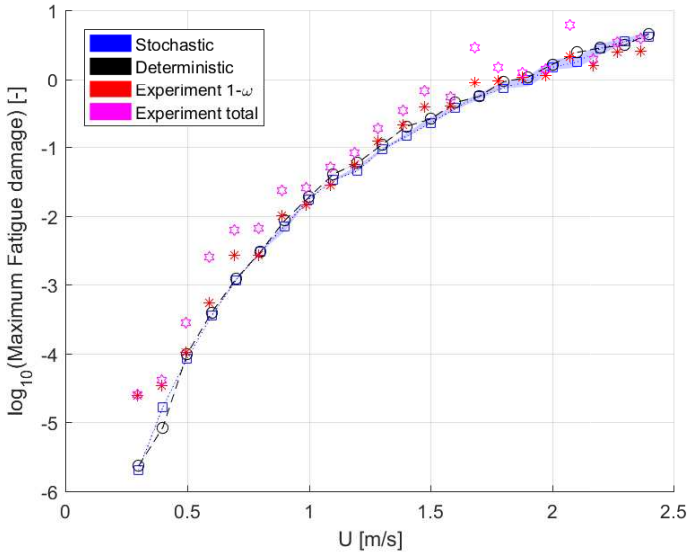

Figure 15: Yearly fatigue damage, sheared flow.

It is to be noted that for a very long time series, the stochastic prediction is also expected to converge towards a specific value of the fatigue damage. Since the steady-state range of the experiment is of limited duration, it is still of interest to see how large scatter is produced by the stochastic model over shorter time durations. In the present analysis, the reported range of simulated results is approximately 225 cycles for each current velocity. Hence, when $N_{split} = 5$, fatigue is calculated for roughly 45 oscillation cycles.

5.3.2. Detailed observations

In the previous section, the proposed prediction tool was verified experimentally in rather general terms. In the following, more detailed verification and discussions are presented by looking into results for particular current speeds, covering a wide range of values. First, the frequency components of cross-flow strain, at the position of maximum r.m.s. strain value, are investigated (figure 16). It is important to note that the Fourier components are found from an equally long time window both for the experiments and the simulations. For the stochastic model, the length of the time window and the randomness in the stochastic synchronization range can affect the power spectrum quite dramatically. Hence, the stochastic result presented in figure 16 is only a realization of a random process. Nevertheless, a general trend is seen. The stochastic model tends to produce a broader frequency spectrum, with less energy at the peak (dominating) frequency, than the deterministic model, which in general agrees better with experimental observations. For low current speeds, the stochastic variation of the synchronization range is unable to reach lock-in with other natural frequencies than what predicted by the deterministic model. Hence, the two models give almost identical predictions for U=0.5 m/s. For moderate and high current velocity (1.5 m/s and 2.4 m/s), a broader range of frequencies are induced in the strain time series due to a constantly changing dominating frequency.

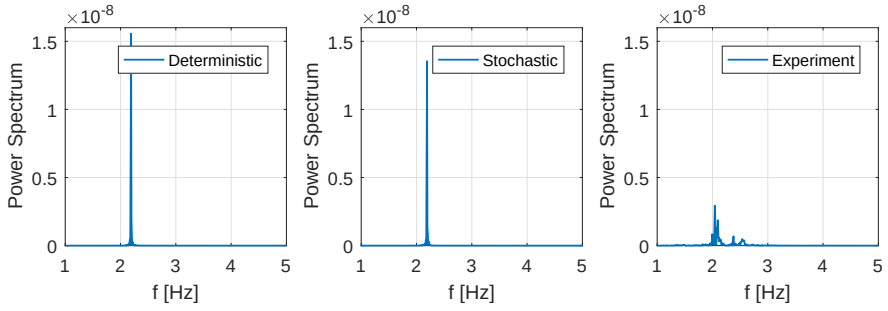

(a) U = 0.5m/s

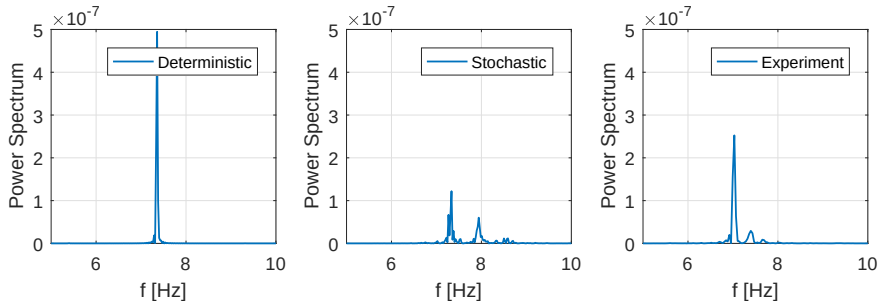

(b) U = 1.5m/s

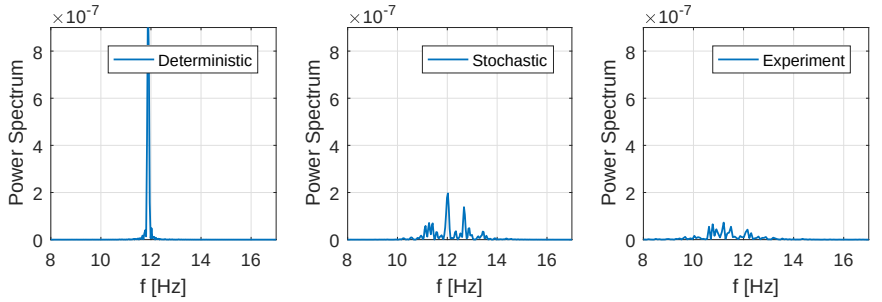

(c) U = 2.4m/s

Figure 16: Power spectrum at measuring position with maximum r.m.s. of strain.

In figure 17, 18 and 19, the predicted and measured strain time series at the same location (i.e. position of maximum r.m.s. value) are presented together with wavelet plots of frequency. It is interesting to look at the

experimental results, where amplitude of vibration and frequency are strongly connected. The amplitudes are severely reduced in time intervals where there is no clear dominating frequency. For other time periods the response is steady-state and amplitudes are high, all in agreement with findings by Modarres-Sadeghi et al. (2011). To exemplify, the low current case (figure 17) shows a shift of dominating frequency at $t \approx 30$s, at the same time as the strain amplitude experiences a sudden and short drop. The rest of the time series is quite stable. For the middle case, i.e. U = 1.5 m/s, the measured strain signal is chaotic between t = 15-25 s, but becomes very steady for the rest of the time window. For U = 2.4 m/s, the response is purely chaotic and the strain signal is strongly amplitude modulated. The stochastic model is able to produce a time variability of frequency which resembles the measurements. However, the amplitude does not display same amount of variation as in the experiment, which contentiously shifts between steady-state and chaotic response. Instead, the stochastic prediction provides a quite stable strain amplitude which might change slightly when a new natural frequency becomes active. The most pronounced changes of amplitude is observed in figure 18, at approximately t = 43 s and t = 54 s. Here, the stochastic model predicts a short time duration with no clear dominating frequency with a resulting drop in amplitude of vibration. This is an indication that the proposed method, to some extent, is able to capture the amplitude modulations associated with chaotic high mode VIV. However, the duration of low amplitude state is shorter than in the experiment, they occur more rarely and they are larger than the lowest values in the measurements. The same can be said about the peaks, at least for the chosen values of $\sigma_{\hat{F}_0\hat{F}_0}$ and c.

Figure 20, 21 and 22 presents the time and space variability of dominating frequencies, for three current velocities. As oppose to the power spectra and wavelet frequency plots, these figures provide additional information about spatial response randomness. The deterministic model shows constant dominating frequency, also in the axial direction, which is consistent with previous findings (figure 12). The stochastic hydrodynamic force model induces a response with clear time variations, but with less degree of spatial variability. However, a change of dominating frequency does not occur at the same time for the whole riser. A shift typically starts where the current is strongest (at $z/L = 0$), and travels towards the opposite pipe end. Hence, for a given time instant, the response might vary as function of z, although the variability follows a clear pattern. The measured frequencies seem to be of a random nature, also in the spatial dimension (see in particular figure 22). Predictions might be improved if the stochastic synchronization was extended to account for axial variations. However, this would violate the strip theory formulation, and complicate the prediction method. Nevertheless, the proposed model reflects the range of measured frequencies quite well.

The longitudinal distributions of fatigue damage at current velocity of 0.5 m/s, 1.5 m/s and 2.4 m/s are presented in figure 23. Same approach as for the fatigue calculations in the previous section is applied. To recall, the total time series of the longitudinal stress was split into $N_{split} = 5$ equally long parts, where fatigue was calculated for each of them. The shadows in figure 23 represent the envelope of these fatigue predictions. Both the deterministic and the stochastic model estimate the damage fairly accurate. The main improvement using stochastic synchronization is the ability to capture parts of the inherent uncertainty of VIV. A general trend is that the deterministic model experiences more pronounced "peaks" and "valleys" in the fatigue distribution, probably because of one dominating mode for the whole simulation time.

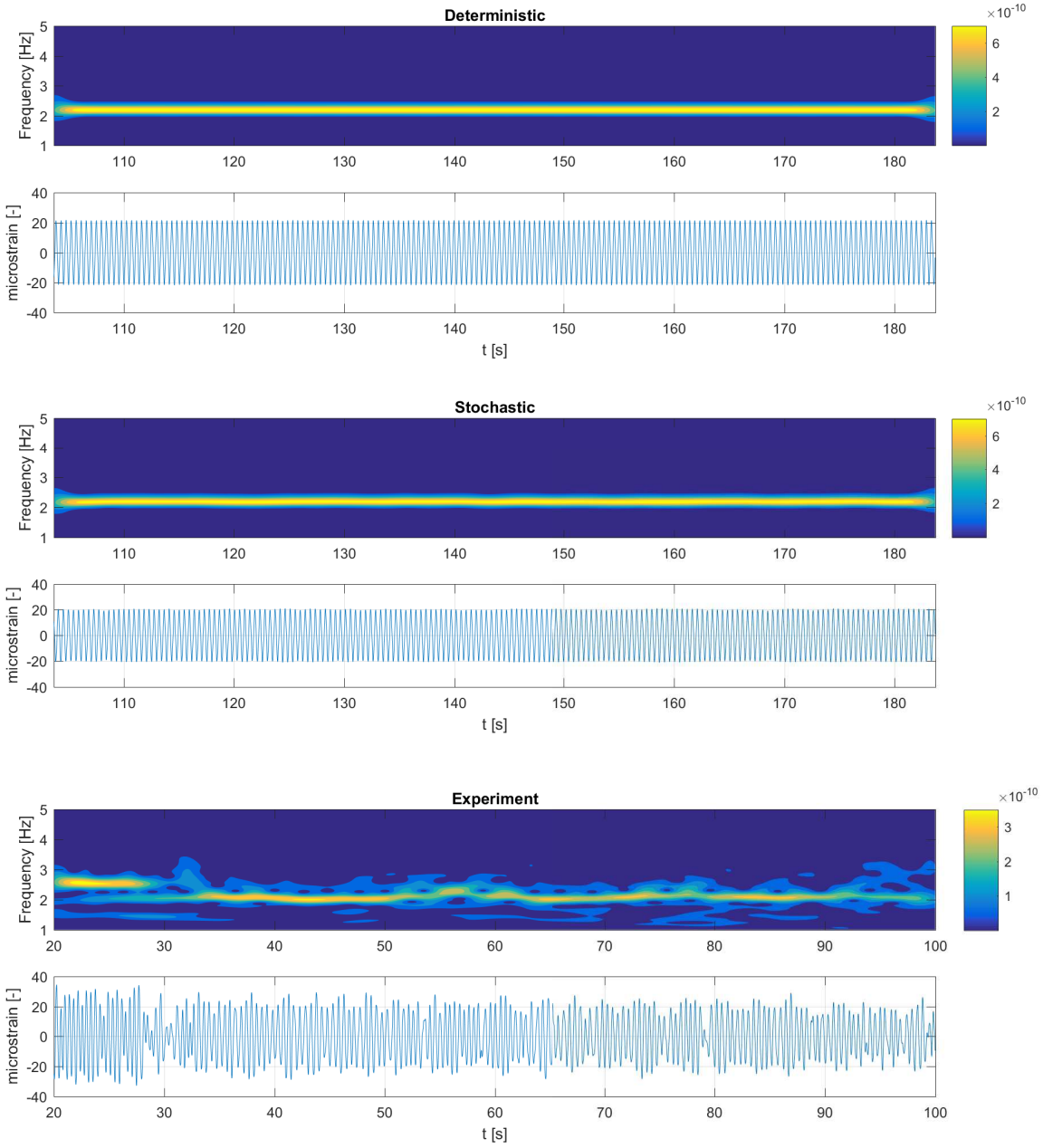

Figure 17: Strain time series and wavelet frequency plot at measuring position with maximum strain r.m.s. value. U=0.5m/s sheared flow.

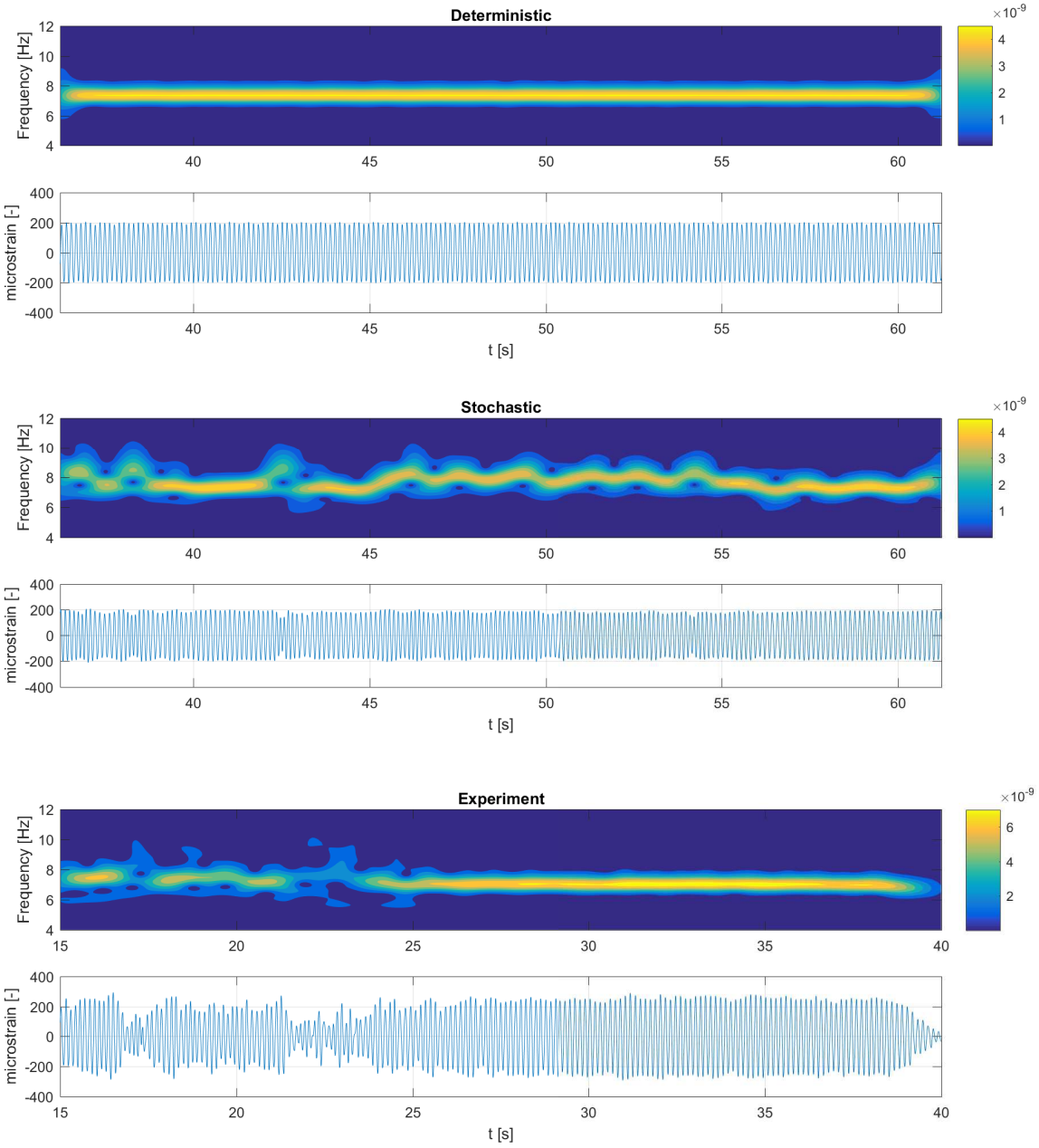

Figure 18: Strain time series and wavelet frequency plot at measuring position with maximum strain r.m.s. value. U=1.5m/s sheared flow.

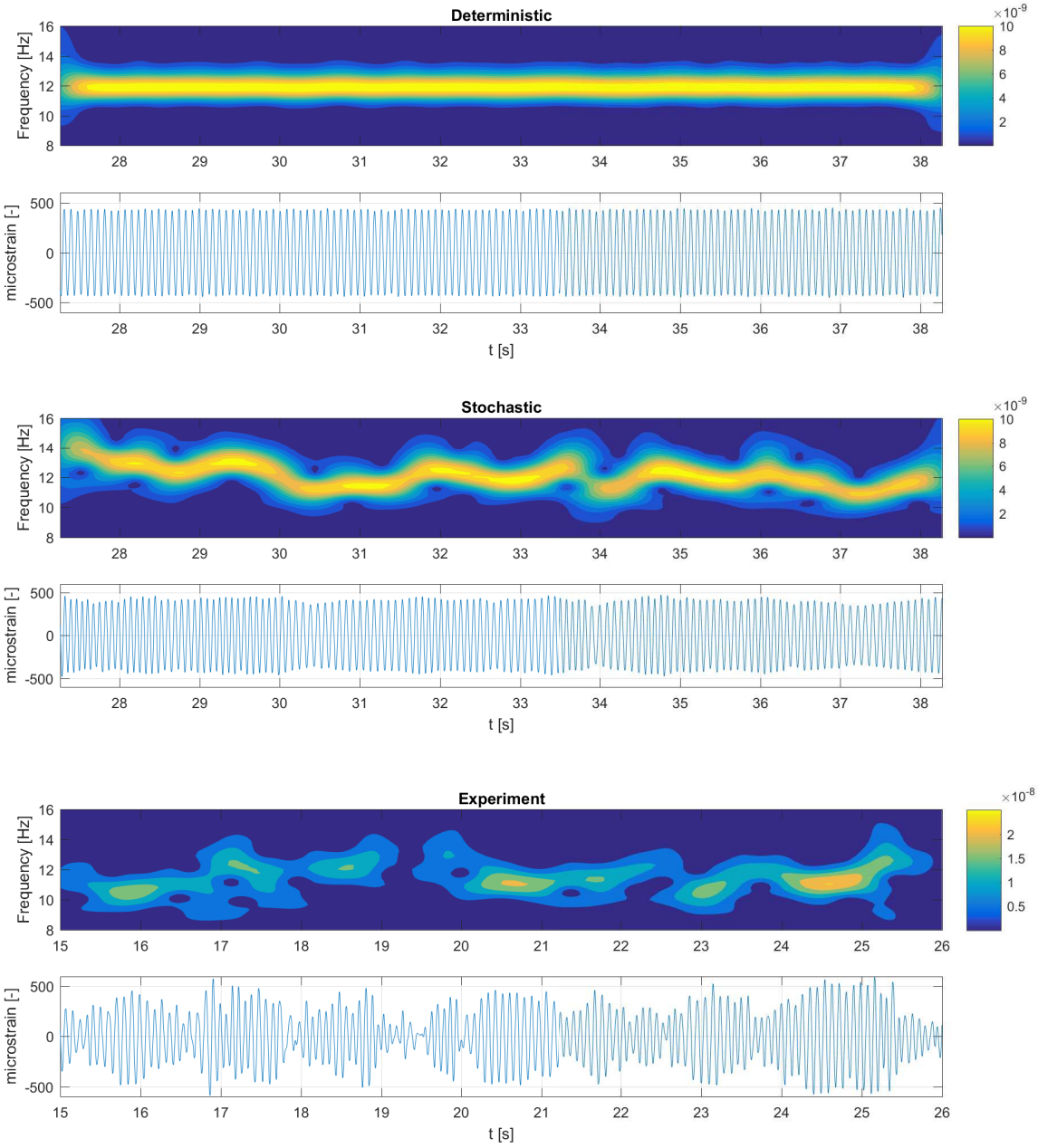

Figure 19: Strain time series and wavelet frequency plot at measuring position with maximum strain r.m.s. value. U=2.4m/s sheared flow.

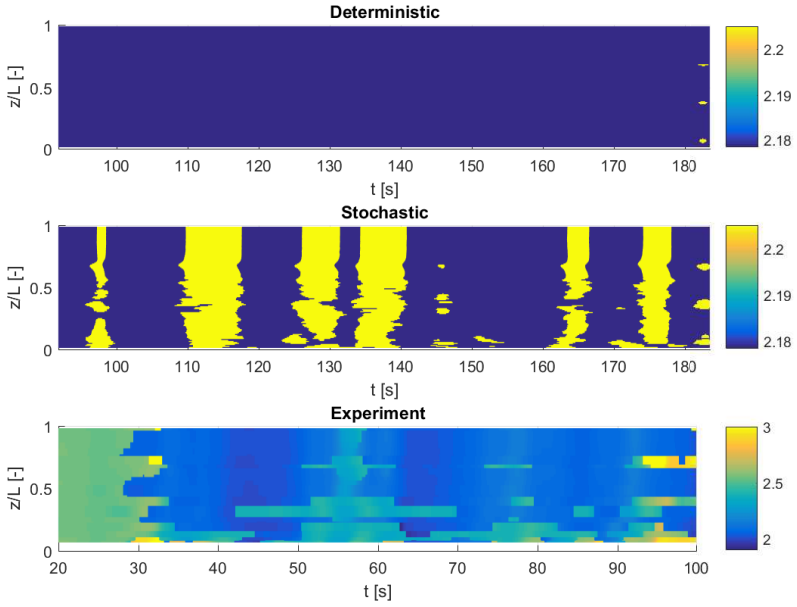

Figure 20: Dominating frequency in Hz as function space and time. The vertical axis is the axial position along riser normalized by pipe length (z/L), and the horizontal axis is time. $U = 0.5$m/s, sheared flow.

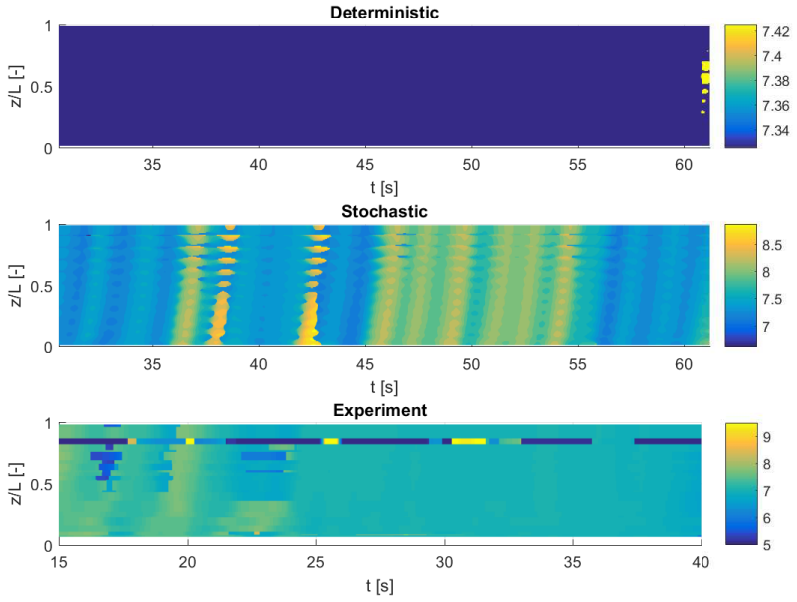

Figure 21: Dominating frequency in Hz as function space and time. The vertical axis is the axial position along riser normalized by pipe length (z/L), and the horizontal axis is time. $U = 1.5$m/s, sheared flow.

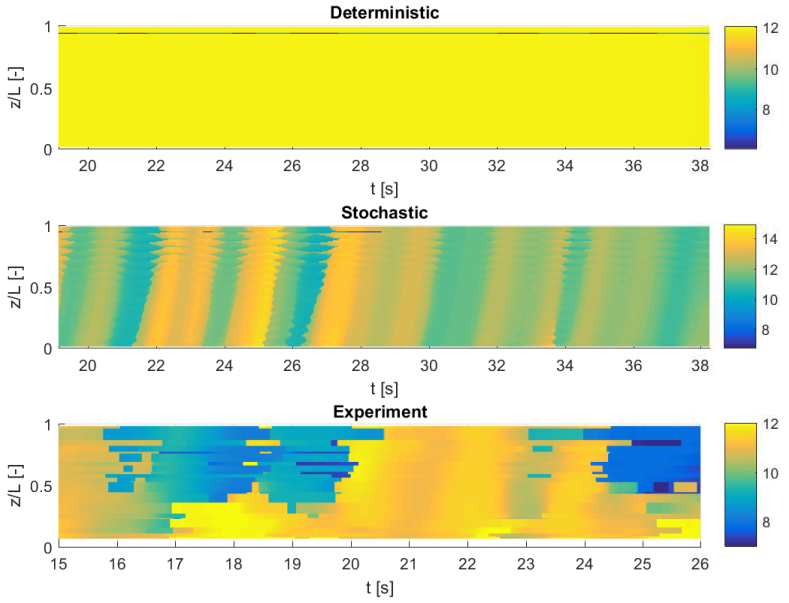

Figure 22: Dominating frequency in Hz as function space and time. The vertical axis is the axial position along riser normalized by pipe length (z/L), and the horizontal axis is time. $U = 2.4$m/s, sheared flow.

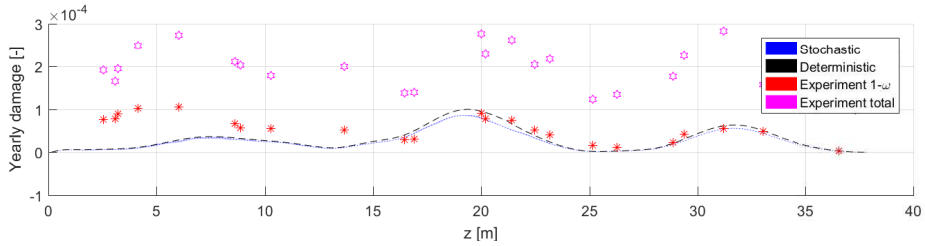

(a) U = 0.5m/s

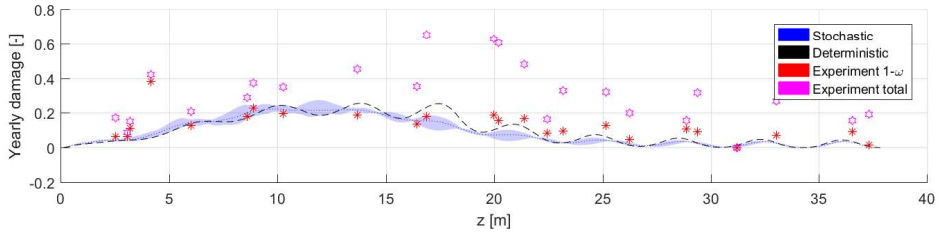

(b) U = 1.5m/s

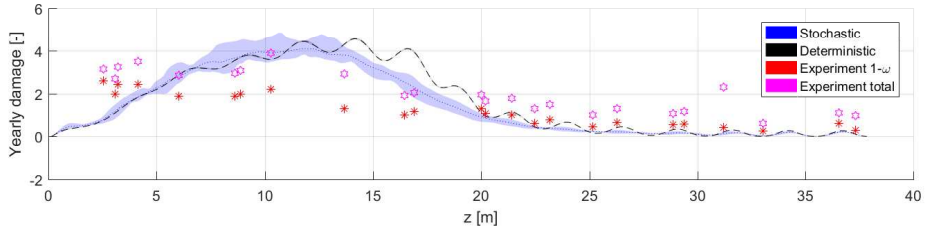

(c) U = 2.4m/s

Figure 23: Longitudinal distribution of accumulated fatigue damage, sheared flow.

5.3.3. Sensitivity study

By choosing $c = 0.07$ and $\sigma_{\hat{F}_0\hat{F}_0} = 0.016$ as the stochastic parameters, the proposed model has demonstrated its ability to provide estimates which on average are close to the deterministic model. Chaotic response is more realistically predicted than before, but some shortcomings are still present. One of these is the model's ability to predict amplitude modulation. Going back to figure 19, the stochastic model displays a time varying frequency, but unlike the experiment, the intensity of the signal is quite constant. In this section $\sigma_{\hat{F}_0\hat{F}_0}$ is increased from 0.016 to 0.040 to investigate if better experimental compliance could be achieved with respect to varying intensity of the signal. Wavelet plots at the riser position with maximum strain r.m.s. are presented for three flow velocities in figure 24. Except for $\sigma_{\hat{F}_0\hat{F}_0}$, all other empirical parameters are the same as before (see table 2).

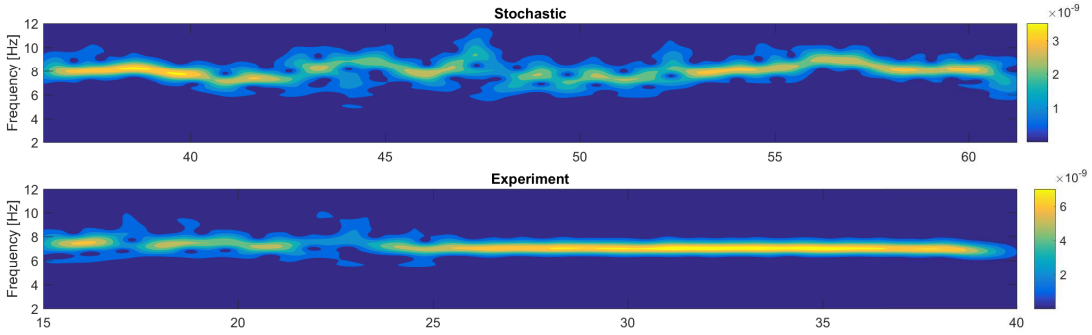

(a) U = 1.5m/s

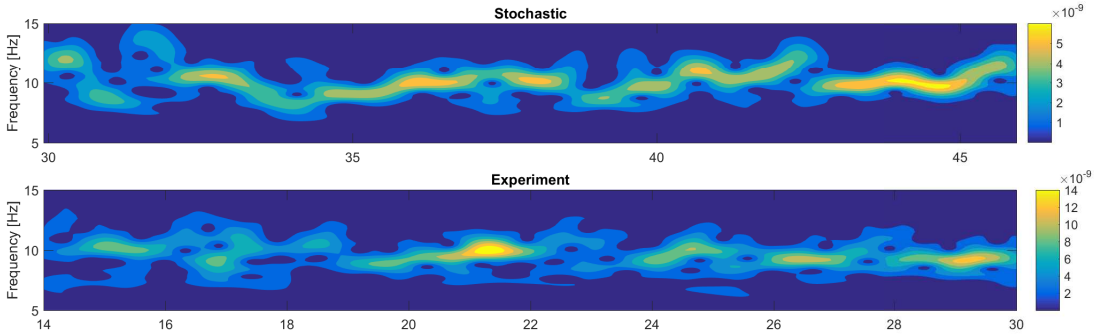

(b) U = 2.0m/s

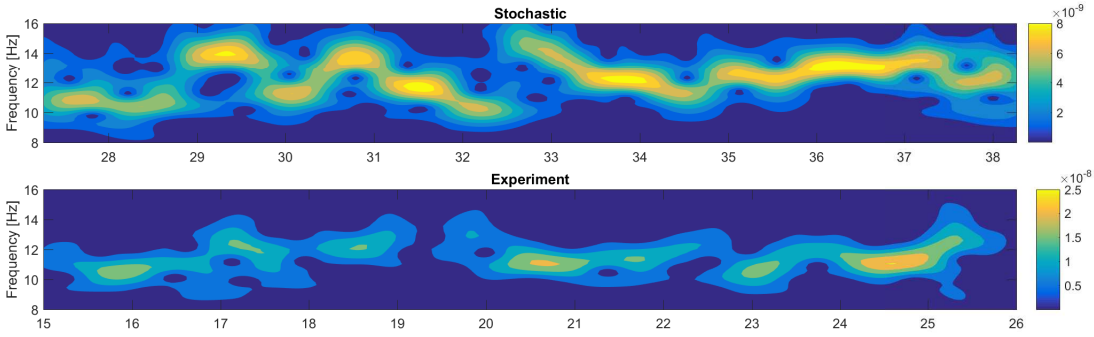

(c) U = 2.4m/s

Figure 24: Wavelet plot showing frequency as function of time at position of maximum strain r.m.s. value, for $\sigma_{\hat{F}_0\hat{F}_0} = 0.040$. All other coefficient are unchanged (see table 2).

The result of a higher standard deviation of $\hat{F}_0$ is that the range of active frequencies increases, but also

that the intensity of the signal is more fluctuating than previously. Looking at figure 24, the stochastic model represents the variability of frequency in a highly realistic way. Still, the experiment gives higher amplitude modulations, but the predictions are significantly improved relative to the original choice of standard deviation (recall figure 18 and 19). However, a change of $\sigma_{\hat{F}_0\hat{F}_0}$ influences not only the frequency, but also the mean amplitude of vibration. Higher standard deviation makes lock-in less obtainable for the riser, so that on average, the response amplitudes drop. To maintain the amplitude level, C_v could be increased. An interesting finding is that the experimental strain signal displays more pronounced amplitude modulations than frequency variations. Hence, to keep increasing $\sigma_{\hat{F}_0\hat{F}_0}$ might not be profitable because the bandwidth of active frequency components will also increase. Probably some sort of stochastic variation of the parameter C_v must be introduced for higher degree of amplitude variation without expanding the range of active frequencies in the strain signal. The other stochastic parameter, i.e. c, was tried doubled to see how the response was affected. No significant effect was observed, indicating that response is more sensitive to $\sigma_{\hat{F}_0\hat{F}_0}$.

6. Conclusion

A new method for stochastic modelling of cross-flow vortex-induced vibrations has been proposed. The work is based on a previously published semi-empirical time domain model which utilized a synchronization algorithm to model lock-in. Synchronization is governed by a constant interval of non-dimensional frequencies, which predicts steady-state response of flexible pipes exposed to time independent currents. The new stochastic feature is to model the midpoint of the synchronization range as a simplified Gaussian process, which on average equals the original proposal by Thorsen et al. (2017). This allows the response of flexible pipes to jump between natural frequencies in the vicinity of what is predicted by the deterministic synchronization algorithm. The range of variability increases as the current velocity is raised.

Through simulation of a long slender riser exposed to sheared flow, the stochastic model has shown to predict reasonable estimates of the measurements. On average, the predictions are close to the deterministic model for same choice of coefficients, as long as the standard deviation is sufficiently low. The main difference is that the deterministic model reach steady-state, whereas variability is demonstrated for the stochastic model. In general, the response becomes more broad banded, with less energy at the peak frequency, which represents the experimental results more realistically. A sensitivity study of the stochastic input to the synchronization model has also been conducted. It indicates that the amplitude modulation associated with chaotic VIV to some extent can be simulated when the standard deviation is sufficiently high. However, it must be kept in mind that the more the Gaussian process deviates from its mean value, the more other properties of the response might be affected. Hence, the empirical coefficients, such as C_v, must be tuned differently than for the deterministic VIV model. Future studies should therefore validate the choice of empirical parameters, to optimize the model performance against measurements. The experiments show clearly that dominating frequency varies both in time and space. The proposed model troubles to predict the spatial variations, which might be a result of the strip theory formulation, or the choice of stochastic coefficients. The simulations were performed using linear finite elements, but it should be tested if a non-linear structural model would amplify the spatial response variability.

As a suggestion for future work, the original model by Thorsen et al. (2017) should be modified to include forcing term(s) for simultaneous cross-flow and in-line VIV (and potentially also pure in-line vibrations (Ulveseter et al., 2017)). The proposed stochastic synchronization might be applied in a similar form as in this paper, to provide realistic randomness in the combined cross-flow and in-line response. However, there are possibilities for further improvements of the stochastic synchronization model. The present work assumes that the random process of synchronization can be applied independently for each structural node. It should be tested if correlation along the riser would improve the performance, such as amplifying the spatial response variability. Experiments have shown that high mode VIV, in some cases, fluctuate between steady-state and chaotic response. When using a high standard deviation for the synchronization algorithm, this paper has shown that a chaotic response is quite realistically predicted. Numerically, it is a simple job to switch between the stochastic and the deterministic synchronization model. However, to quantify "when" and "for how long" the two different response types should be simulated is a challenging task. For better modelling of amplitude modulations the vortex shedding force coefficient C_v could be made a stochastic process.

7. Acknowledgement

Thanks to Jie Wu for wavelet subroutines used to find dominating frequency as function of time and space, and to Norwegian Deepwater Programme (NDP) for providing experimental data.

8. References

Baarholm, G., Larsen, C., Lie, H., 2006. On fatigue damage accumulation from in-line and cross-flow vortex-induced vibrations on risers. Journal of Fluids and Structures 22 (1), 109–127.

Braaten, H., Lie, H., 2005. NDP Riser High Mode VIV Tests Main Report. Tech. rep., Norwegian Marine Technology Research Institute.

Brunborg, M., 2013. Vortex Induced Vibrations of Slender Marine Structures. M.sc. thesis, Norwegian University of Science and Technology.

DNV GL, 2014. Recommeded Practice DNVGL-RP-0005:2014-06 RPC203: Fatigue design of offshore steel structures. Tech. rep.

Fergestad, D., Løtveit, S. A., 2014. Handbook on Design and Operation of Flexible Pipes.

Gopalkrishnan, R., 1993. Vortex-Induced Forces on Oscillating Bluff Cylinders. Ph.D. thesis, Massachusetts Institute of Technology (MIT).

Kristiansen, T., Lie, H., 2005. NDP Riser High Mode VIV Tests - Modal Analysis. Tech. rep., Norwegian Marine Technology Research Institute.

Langen, I., Sigbjoernsson, R., 1979. Dynamisk analyse av konstruksjoner (Dynamic Analysis of Structures). Tapir.

Lie, H., Larsen, C. M., Kaasen, K. E., 2008. Frequency Domain Model for Prediction of Stochastic Vortex Induced Vibrations for Deep Water Risers. In: Proceedings of the ASME 27th International Conference on Offshore Mechanics and Arctic Engineering.

Modarres-Sadeghi, Y., Chasparis, F., Triantafyllou, M., Tognarelli, M., Beynet, P., 2011. Chaotic response is a generic feature of vortex-induced vibrations of flexible risers. Journal of Sound and Vibration 330 (11), 2565–2579.

Mukundan, H., Modarres-Sadeghi, Y., Dahl, J., Hover, F., Triantafyllou, M., 2009. Monitoring VIV fatigue damage on marine risers. Journal of Fluids and Structures 25 (4), 617–628.

Øritsland, O., 2004. Ormen Lange VIV Model Tests Phase III. Tech. rep., Norwegian Marine Technology Research Institute.

Passano, E., Larsen, C. M., Lie, H., Wu, J., 2014. Vivana Theory Manual. Tech. rep.

Sarpkaya, T., may 2004. A critical review of the intrinsic nature of vortex-induced vibrations. Journal of Fluids and Structures 19 (4), 389–447.

Swithenbank, S. B., 2007. Dynamics of Long Flexible Cylinders at High-Mode Number in Uniform and Sheared Flows. Ph.D. thesis, Massachusetts Institute of Technology.

Swithenbank, S. B., Larsen, C. M., 2012. Occurrence of High Amplitude VIV with Time Sharing. In: Proceedings of the ASME 2012 31st International Conference on Ocean, Offshore and Arctic Engineering.

Thorsen, M., Sævik, S., Larsen, C., 2014. A simplified method for time domain simulation of cross-flow vortex-induced vibrations. Journal of Fluids and Structures 49, 135–148.

Thorsen, M., Sævik, S., Larsen, C., feb 2016. Time domain simulation of vortex-induced vibrations in stationary and oscillating flows. Journal of Fluids and Structures 61, 1–19.

Thorsen, M., Sævik, S., Larsen, C., 2017. Non-linear time domain analysis of cross-flow vortex-induced vibrations. Marine Structures 51, 134–151.

Thorsen, M. J., Sævik, S., Larsen, C. M., 2015. Fatigue damage from time domain simulation of combined in-line and cross-flow vortex-induced vibrations. Marine Structures 41, 200–222.

Ulveseter, J., Sævik, S., Larsen, C., 2017. Time domain model for calculation of pure in-line vortex-induced vibrations. Journal of Fluids and Structures 68, 158–173.

Vandiver, J. K., Li, L., 2005. SHEAR7 V4.4 PROGRAM THEORETICAL MANUAL. Tech. rep., Department of Ocean Engineering Massachusetts Institute of Technology.

Vikestad, K., Vandiver, J., Larsen, C., 2000. Added mass and oscillation frequency for a circular cylinder subjected to vortex-induced vibrations and external disturbance. Journal of Fluids and Structures 14 (7), 1071–1088.

Wang, J., Fu, S., Baarholm, R., Wu, J., Larsen, C. M., 2014. Fatigue damage of a steel catenary riser from vortex-induced vibration caused by vessel motions. Marine Structures 39, 131–156.

Wu, X., Ge, F., Hong, Y., 2012. A review of recent studies on vortex-induced vibrations of long slender cylinders. Journal of Fluids and Structures 28, 292–308.